Neuron, Vol. 44, 483–493, October 28, 2004, Copyright ©2004 by Cell Press

State-Dependent Calcium Signaling in Dendritic Spines of Striatal Medium Spiny Neurons

Adam G. Carter and Bernardo L. Sabatini*
Department of Neurobiology
Harvard Medical School
220 Longwood Avenue
Boston, Massachusetts 02115

Summary

Striatal medium spiny neurons (MSNs) in vivo undergo large membrane depolarizations known as state transitions. Calcium (Ca) entry into MSNs triggers diverse downstream cellular processes. However, little is known about Ca signals in MSN dendrites and spines and how state transitions influence these signals. Here, we develop a novel approach, combining 2-photon Ca imaging and 2-photon glutamate uncaging, to examine how voltage-sensitive Ca channels (VSCCs) and ionotropic glutamate receptors contribute to Ca signals in MSNs. We find that upstate transitions switch the VSCCs available in dendrites and spines, decreasing T-type while enhancing L-type channels. Moreover, these transitions change the dominant synaptic Ca source from Ca-permeable AMPA receptors to NMDA receptors. Finally, pairing bAPs with synaptic inputs generates additional synaptic Ca signals due to enhanced Ca influx through NMDA receptors. By altering the sources, amplitude, and kinetics of spine Ca signals, state transitions may gate synaptic plasticity and gene expression in MSNs.

Introduction

The striatum is the input stage of the basal ganglia and its function is necessary for the generation and control of voluntary movements (Wilson, 1998). The principal cell of the striatum is the medium spiny neuron (MSN), which receives strong glutamatergic input from cortex and thalamus onto its dendritic spines and sends GABAergic projections to globus pallidus and substantia nigra. The importance of MSNs is highlighted by the profound motor deficits found in Huntington's and Parkinson's diseases, which are characterized by degeneration or deregulation of MSNs. In vivo, the output of the striatum is shaped by the intrinsic membrane properties of MSNs, whose membrane potential exhibits transitions from a resting "downstate" near −80 mV to a depolarized "upstate" near −50 mV (Wilson and Kawaguchi, 1996). Action potentials (APs) are fired from the upstate, and thus state transitions are thought to modulate basal ganglia function by enabling striatal output (Stern et al., 1998).

MSNs express a wide array of conductances whose properties are likely modulated by the large changes in resting potential that accompany state transitions (Wilson, 1998). These conductances include voltage-sensitive sodium and potassium channels, many classes of low- and high-threshold voltage-sensitive calcium (Ca) channels (VSCCs), and ionotropic glutamate receptors. Multiple neuronal processes in MSNs are regulated by Ca influx, including synaptic strength (Calabresi et al., 1992; Partridge et al., 2000) and gene expression (Konradi et al., 1996; Liu and Graybiel, 1996; Rajadhyaksha et al., 1999). MSNs may possess routes for Ca entry not found in other principal neurons, including Ca-permeable AMPA receptors (AMPARs) (Bernard et al., 1997; Chen et al., 1998; Stefani et al., 1998). Moreover, Ca sources may be preferentially activated in the two states, such as T-type VSCCs capable of activating at relatively hyperpolarized potentials (McRory et al., 2001). However, little is known about subcellular Ca signals in MSNs and how they are influenced by state transitions.

In cultured MSNs, upstate transitions are triggered by spontaneous synaptic inputs and can generate dendritic Ca signals (Kerr and Plenz, 2002) that are enhanced by back-propagating APs (bAPs) (Kerr and Plenz, 2004). However, assessing which VSCCs and glutamate receptors contribute to these Ca signals is difficult, as blocking them also disrupts the generation of upstates (Plenz and Kitai, 1998; Vergara et al., 2003). In other central neurons, complex interactions between synaptic inputs and active conductances shape Ca signals in dendrites and spines (Koester and Sakmann, 1998; Magee and Johnston, 1997; Waters et al., 2003; Yuste and Denk, 1995). Thus, synaptic inputs evoke depolarizations that can open VSCCs or enhance their opening by bAPs (Denk et al., 1995; Reid et al., 2001; Schiller et al., 1998). Moreover, depolarization during bAPs may augment Ca influx through NMDA receptors (NMDARs) via relief of extracellular magnesium block (Nevian and Sakmann, 2004). However, determining the role of active conductances in these interactions is generally difficult, because blocking these channels also interferes with presynaptic release of glutamate.

Here we assess how state transitions alter both bAP- and synaptic-Ca signals in MSN dendrites and spines from acute rat striatal slices. Our results indicate that subthreshold depolarization changes the available VSCCs from T- and R-type to L- and R-type. We develop a novel imaging approach to study synaptic Ca signals, combining 2-photon laser-scanning microscopy (2PLSM) and 2-photon laser uncaging (2PLU) of glutamate. This approach allows us to activate postsynaptic glutamate receptors at single synapses while simultaneously monitoring evoked Ca signals in dendrites and spines. By circumventing presynaptic glutamate release, this method permits a mechanistic analysis of how active conductances and glutamate receptors contribute to synaptic Ca signals. We find that synaptic Ca signals in the downstate are dominated by Ca-permeable AMPARs. However, subthreshold depolarization switches the dominant source of Ca from AMPARs to NMDARs. Finally, pairing bAPs and synaptic inputs in the upstate further enhances synaptic Ca signals by increasing Ca influx via NMDARs. Thus, in addition to shaping the output of the striatum, state transitions influence synaptic inputs and regulate Ca signals within dendrites and spines, which

*Correspondence: bernardo_sabatini@hms.harvard.edu

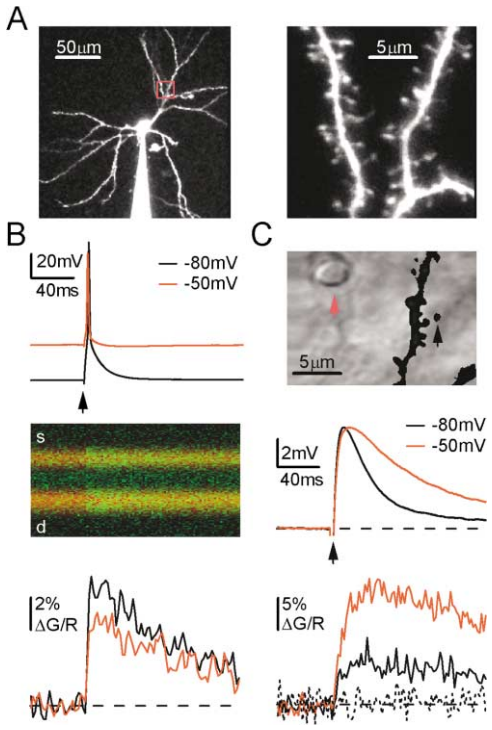

Figure 1. Subthreshold Depolarization Regulates bAP- and Synaptic-Ca Signals in Spines and Dendrites

(A) 2PLSM images of a MSN, showing the whole neuron (left) and a segment of spiny dendrites (right). Fluorescence from the red channel is shown.

(B) Line scans reveal that somatically generated bAPs (top) evoke fluorescence transients in both the spine head (s) and parent dendrite (d) (middle). Bottom: Quantification of the fluorescence transients indicates that the bAP Ca signal in the spine head is smaller when the neuron rests at −50 mV (red) than at −80 mV (black).

(C) Top: Overlaid 2PLSM and laser-scanning IR-DIC images of a segment of spiny dendrites and an extracellular stimulus electrode (red arrow) near the spine containing a stimulated synapse (black arrow). Middle: Stimulation of afferent input leads to a broader EPSP at −50 mV (red) than at −80 mV (black). Bottom: Fluorescence transients recorded from the indicated spine (solid lines) and neighboring dendrite (dashed line) show that the synaptic Ca signal is limited to the spine head and is larger at −50 mV (red) than at −80 mV (black).

may gate the activation of downstream Ca-dependent processes.

Results

Subthreshold Depolarization Alters bAP- and Synaptic-Ca Signals

We studied Ca signals in dendrites and spines of MSNs in acute slices from rat dorsal striatum (Figure 1). MSNs were filled through a whole-cell recording pipette with a green-fluorescing Ca indicator and a red-fluorescing morphological marker. 2-photon laser scanning microscopy (2PLSM) revealed cells with small somas and thin branching dendrites studded with spines (Figure 1A). A brief depolarizing current injection at the soma triggered a back-propagating action potential (bAP) that evoked an increase in green fluorescence, indicative of Ca entry ($\Delta[Ca]_{bAP}$) into spines and dendrites (Figure 1B). Ca imaging was performed under conditions in which changes in green fluorescence normalized to the red fluorescence ($\Delta G/R$) are linearly proportional to Ca influx (Sabatini et al., 2002; see Experimental Procedures). bAP fluorescence signals ($\Delta G/R_{bAP}$) had a rapid rising phase (<4 ms) and were blocked by 1 μM TTX ($\Delta G/R_{bAP}$ = 2% ± 7% of control in dendrites and 1% ± 2% in spines; n = 4 cells, 4 spines), consistent with bAPs activating direct Ca influx through VSCCs.

Endogenous Ca buffers are intracellular Ca binding proteins that influence the amplitude and kinetics of intracellular Ca signals. Using $\Delta G/R_{bAP}$ measurements, we calculated the endogenous Ca buffer capacity (K_E) of MSNs (see Experimental Procedures and Supplemental Figure S1A at http://www.neuron.org/cgi/content/full/44/3/483/DC1/), giving values of 96 (38–146, 95% confidence interval) in dendrites and 84 (62–137) in spines. These values are intermediate to those found in interneurons (140) (Goldberg et al., 2003; Lee et al., 2000) and pyramidal neuron dendrites (50–200) (Helmchen et al., 1996; Lee et al., 2000; Maravall et al., 2000) and spines (25) (Sabatini et al., 2002), but much lower than those reported for other spiny inhibitory projection neurons (2000) (Fierro and Llano, 1996). Thus, in intact MSNs dendrites and spines without the added Ca buffer introduced by Ca indicator, $\Delta[Ca]_{bAP}$ is expected to reach ~400 nM and clear with a decay time constant of ~25 ms.

Somatic recordings have demonstrated several classes of VSCCs in MSNs (Bargas et al., 1994; Hoehn et al., 1993) whose gating properties may be sensitive to the depolarization that accompanies upstate transitions. We assessed the influence of subthreshold depolarization on $\Delta[Ca]_{bAP}$ in spines and dendrites (Figure 1B). $\Delta G/R_{bAP}$ was monitored in the spine head and neighboring dendrite when the neuron was resting at −80 mV ($\Delta G/R_{bAP}^{-80mV}$) or depolarized to −50 mV ($\Delta G/R_{bAP}^{-50mV}$) via the somatic recording pipette (100–200 pA current injection). On average, the ratio of $\Delta G/R_{bAP}^{-50mV}$ to $\Delta G/R_{bAP}^{-80mV}$ ($R_{\Delta G/R,bAP}^{-50/-80mV}$) in spines and dendrites was 0.82 ± 0.03 and 0.82 ± 0.04, respectively, and was significantly less than unity (n = 10 cells, 15 spines). There was no dependence on the distance from the soma for either $\Delta G/R_{bAP}^{-80mV}$ or $\Delta G/R_{bAP}^{-50mV}$ (Supplemental Figure S1B). Thus, somatic depolarization can influence $\Delta[Ca]_{bAP}$ and may alter the activation of voltage-gated conductances within spines and dendrites.

MSNs receive excitatory inputs from the cortex and thalamus onto their dendritic spines and have both AMPAR- and NMDAR-mediated synaptic responses. To examine the effects of subthreshold depolarization on synaptic responses, small stimulus electrodes were used to activate presynaptic axons near a spiny stretch of dendrites of a MSN held in current clamp in the presence of mGluR blockers (Figure 1C). The EPSP amplitude was similar at −80 mV and −50 mV (6.6 ± 1.2 versus 6.2 ± 1.1 mV; n = 6 cells, 9 spines), but the half-decay time was increased by depolarization (22 ± 3 versus 46 ± 7 ms). Are these changes in the kinetics of the EPSP accompanied by changes in synaptic Ca signals ($\Delta[Ca]_{syn}$) in spines? In the same experiments, 2PLSM was used to identify a spine head containing an activated synapse and monitor synaptic fluorescence transients ($\Delta G/R_{syn}$). In contrast to bAP Ca signals,

$\Delta[Ca]_{syn}$ was restricted to the spine head with little Ca accumulation in the dendritic shaft. Moreover, $\Delta[Ca]_{syn}$ was long lasting, with $\Delta G/R_{syn}^{-80mV}$ peaking in 55 ± 20 ms and remaining elevated for hundreds of milliseconds. The amplitude of $\Delta[Ca]_{syn}$ was also sensitive to subthreshold depolarization, such that $R_{\Delta G/R,syn}^{-50/-80mV}$ was 2.80 ± 0.4. Thus, in contrast to its effects on bAP Ca signals, subthreshold depolarization greatly enhances $\Delta[Ca]_{syn}$ in activated spines.

Subthreshold Depolarization Alters VSCC Availability

The dependence of $\Delta[Ca]_{bAP}$ and $\Delta[Ca]_{syn}$ on resting membrane potential might reflect differential activation of VSCC classes at −80 mV and −50 mV. Different VSCCs are selectively coupled to distinct intracellular signaling cascades, including kinase activation (Yasuda et al., 2003) and gene transcription (Liu and Graybiel, 1996). To assess how subthreshold depolarization changes the contribution of different VSCCs to $\Delta[Ca]_{bAP}$, $R_{\Delta G/R,bAP}^{-50/-80mV}$ was measured in the presence of class-specific VSCC antagonists (Figure 2A). The T-type blocker Ni^{2+} (50 μM) significantly increased $R_{\Delta G/R,bAP}^{-50/-80mV}$ to 0.94 ± 0.04 in spines and 0.98 ± 0.05 in dendrites (n = 13 cells, 15 spines), consistent with greater activation of these low-voltage activated channels at hyperpolarized potentials. The R-type blocker SNX-482 (0.3 μM; n = 7 cells, 10 spines) and N/P/Q-type blocker ω-conotoxin-MVIIC (1 μM; n = 8 cells, 9 spines) did not significantly change $R_{\Delta G/R,bAP}^{-50/-80mV}$, consistent with either negligible or similar activation at the two potentials. The L-type blocker nimodipine (20 μM; n = 6 cells, 8 spines) significantly reduced $R_{\Delta G/R,bAP}^{-50/-80mV}$, consistent with greater activation at depolarized potentials. Finally, a similar decrease in $R_{\Delta G/R,bAP}^{-50/-80mV}$ was seen with mibefradil (20 μM; n = 8 cells, 9 spines), which at these concentrations blocks both T-type and L-type channels (Jimenez et al., 2000). These results suggest differential activation of T- and L-type channels by bAPs in down- and upstates.

The effects of each antagonist on $R_{\Delta G/R,bAP}^{-50/-80mV}$ implicate differential activation of VSCC classes but cannot identify whether activation of a given channel is increased at one potential or decreased at the other. Thus, we directly assessed the contribution of different VSCC classes to $\Delta[Ca]_{bAP}$ at each potential by locally applying VSCC blockers to the visualized spine with a puffing pipette, which allows us to rapidly block VSCCs within the slice (Figure 2B). A cocktail of VSCC blockers (referred to below as the VSCC cocktail), consisting of SNX-482, ω-conotoxin-MVIIC, nimodipine, and mibefradil, effectively blocked $\Delta G/R_{bAP}$ both at resting potentials of −80 mV (n = 4 cells, 5 spines) (Figures 2B and 2C) and in MSNs depolarized to −50 mV (n = 5 cells, 5 spines) (Figure 2C). At −80 mV, Ni^{2+} (n = 6 cells, 6 spines), SNX-482 (n = 4 cells, 4 spines), and mibefradil (n = 5 cells, 6 spines) significantly reduced $\Delta G/R_{bAP}^{-80mV}$, whereas ω-conotoxin-MVIIC (n = 5 cells, 5 spines) and nimodipine (n = 6 cells, 6 spines) had no effect (Figure 2C). In contrast, at −50 mV, SNX-482 (n = 5 cells, 5 spines), nimodipine (n = 5 cells, 5 spines), and mibefradil (n = 5 cells, 5 spines) significantly reduced $\Delta G/R_{bAP}^{-50mV}$, while Ni^{2+} (n = 5 cells, 6 spines) caused a small decrease and ω-conotoxin-MVIIC (n = 5 cells, 5 spines) had no

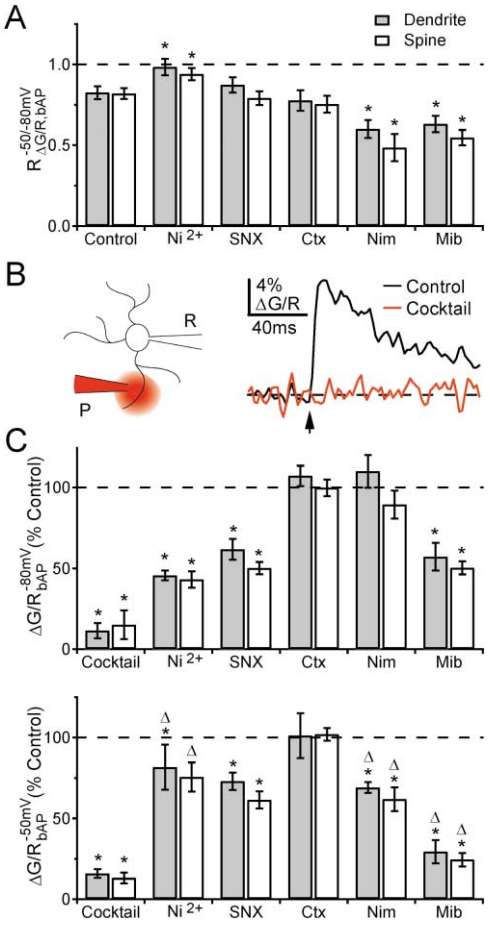

Figure 2. Subthreshold Depolarization Alters Voltage-Sensitive Ca Channels Activated by bAPs

(A) Ratio of the amplitudes of bAP Ca signals at −50 and −80 mV measured in spine heads and dendrites in control conditions and in the presence of Ni^{2+}, SNX-482, ω-conotoxin-MVIIC (Ctx), nimodipine (Nim), or mibefradil (Mib). Asterisk indicates significant difference from control conditions.

(B) Left: Schematic illustrating local application of drugs via a puffer pipette (P) placed near the recording pipette (R) in the dendritic region containing the analyzed spine. Right: Local application of the VSCC cocktail blocks $\Delta G/R_{bAP}$.

(C) Summary of the effects of local application of VSCC antagonists on $\Delta G/R_{bAP}$ in spines and dendrites of MSNs resting at −80 mV (top) or −50 mV (bottom). Asterisk indicates significant difference from unity, and triangle indicates values at −50 mV that are significantly different from those at −80 mV.

effect (Figure 2C). The Ni^{2+} block was significantly less at −50 mV than at −80 mV, whereas the nimodipine and mibefradil block was significantly greater, and the SNX-482 and ω-conotoxin-MVIIC block was similar (Figure 2C). These results indicate that multiple VSCC classes can contribute to evoked Ca signals in MSN dendrites and spines, including L-type channels not activated by single bAPs in hippocampal pyramidal neurons (Sabatini and Svoboda, 2000; Yasuda et al., 2003). Moreover, depolarization within the subthreshold range alters the complement of active VSCCs in MSN dendrites and spines, from T- and R-type channels in the downstate to L- and R-type channels in the upstate.

Combined 2PLSM and 2PLU Used to Study Synaptic Ca Signals in Spines

Differential activation of voltage-sensitive conductances, including Na and Ca channels, may also contribute to the effects of subthreshold depolarization on $\Delta[Ca]_{syn}$ within the spine head seen in Figure 1. Alternatively, depolarization may directly modulate Ca influx through AMPARs and NMDARs. Distinguishing between these possibilities is difficult for several reasons when synapses are activated using extracellular stimulation of axons. First, pharmacological analysis of the role of dendritic voltage-sensitive conductances is limited because blocking Na or Ca channels alters or prevents glutamate release. Second, the number of activated synapses and their spatial arrangement are difficult to control and monitor, and these factors may influence the recruitment of dendritic conductances. Third, selection of synapses for analysis is biased toward those that evoke large Ca signals with low presynaptic failure rates. Finally, stimulation of local GABAergic and cholinergic interneurons or dopaminergic fibers in the striatum can have heterosynaptic effects on glutamate release and postsynaptic responses.

We studied $\Delta[Ca]_{syn}$ by combining 2PLSM with simultaneous 2-photon laser uncaging (2PLU) of MNI-glutamate (Figure 3). This method allowed us to mimic synaptic inputs and measure $\Delta G/R_{syn}$ in spines without stimulating presynaptic glutamate release. We found that 2PLU with brief laser pulses (0.5 ms) at 720 nm evoked inward currents in the postsynaptic cell (Figure 3A), as previously demonstrated in pyramidal neurons (Matsuzaki et al., 2001; Smith et al., 2003). These uncaging-evoked excitatory currents (UECs) had rapid kinetics closely matching those of miniature EPSCs (mEPSCs) recorded in the same cells. On average, the amplitude and decay of UECs were 18 $\pm$ 2 pA and 8.6 $\pm$ 0.7 ms, while those of mEPSCs were 11 $\pm$ 1 pA and 8.4 $\pm$ 1.7 ms (n = 4 cells, 5 spines). The UEC amplitude is determined by the laser power and uncaging pulse duration (Figure 3B) and was empirically set in our experiments to be within the range of mEPSC amplitudes (peak mEPSC amplitudes were 35 $\pm$ 4 pA). We found that combining 2PLSM and 2PLU made it possible to study $\Delta[Ca]_{syn}$ in adjacent spines separated by only a few microns, such that uncaging onto one spine evoked a Ca signal only in that spine (Figure 3C). These results confirm the spatial localization of excitation and are consistent with previous results using 2PLU to map postsynaptic receptors (Matsuzaki et al., 2001, 2004). Importantly, neither UECs nor $\Delta[Ca]_{syn}$ were observed when MNI-glutamate was not present. Together, these results demonstrate that combined 2PLSM and 2PLU can be used to mimic synaptic inputs and study $\Delta[Ca]_{syn}$ in single spines while avoiding the limitations of electrical stimulation.

Synaptic responses evoked by glutamate uncaging were influenced by subthreshold depolarization in a similar manner to electrically evoked responses. The uncaging-evoked excitatory potential (UEP) amplitude was similar at -80 mV and -50 mV (0.6 $\pm$ 0.1 versus 0.6 $\pm$ 0.1 mV; n = 6 cells, 9 spines), whereas the half-decay time was prolonged at -50 mV (15 $\pm$ 1 versus 39 $\pm$ 6 ms) (Figure 3D). Moreover, the concomitant $\Delta[Ca]_{syn}$ was increased by depolarization ($R^{-50/-80mV}_{\Delta G/R,syn}$ was 2.4 $\pm$ 0.2; n = 7 cells, 12 spines). To assess the role of active dendritic conductances to the enhancement of $\Delta[Ca]_{syn}$, we eliminated contributions from voltage-sensitive Na and Ca channels by including TTX and the VSCC cocktail in the bath. Under these conditions, the UEP amplitude was larger at -80 mV than -50 mV (0.7 $\pm$ 0.2 versus 0.4 $\pm$ 0.1 mV; n = 4 cells, 8 spines) and the half-decay time was similar (20 $\pm$ 4 versus 15 $\pm$ 3 ms). However, subthreshold depolarization continued to increase $\Delta[Ca]_{syn}$ in spines ($R^{-50/-80mV}_{\Delta G/R,syn}$ was 2.6 $\pm$ 0.4; n = 4 cells, 8 spines) (Figure 3E). Thus, while active Na and Ca con-

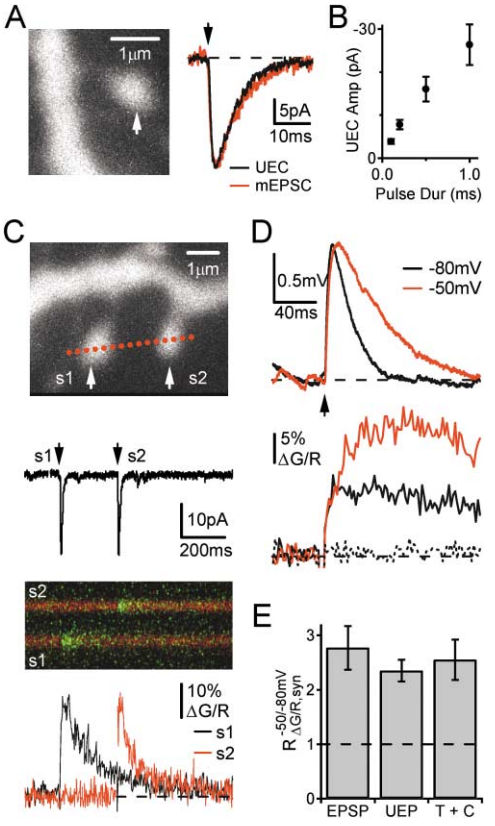

Figure 3. Stimulation of Synapses with 2-Photon Laser Uncaging of Glutamate and Simultaneous 2PLSM of Evoked Ca Signals

(A) Left: 2PLSM image of a spine head and parent dendrite, with arrow indicating the uncaging position. Right: Average UEC (black) evoked by a 0.5 ms uncaging pulse (arrow), compared to the peak-scaled average mEPSC (red) from the same cell.

(B) UEC amplitude (amp) plotted against uncaging pulse duration (dur).

(C) Top: 2PLSM image of two closely spaced spines (s1 and s2). Middle: UECs evoked by uncaging pulses (black arrows) at s1 and s2 (white arrows in top). Bottom: Fluorescence transients collected simultaneously in line scan mode (red line in top), aligned with the voltage-clamp recording, show that uncaging evokes a Ca signal that is restricted to the stimulated spine head.

(D) Top: UEPs are broader at -50 mV (red) than at -80 mV (black). Bottom: Simultaneously recorded fluorescence transients from a single spine head (solid lines) and neighboring dendrite (dashed line) indicate that synaptic Ca signals are larger at -50 mV (red) than at -80 mV (black).

(E) Summary of the fractional increase in $\Delta G/R_{syn}$ following depolarization to -50 mV when axonal fibers are stimulated electrically (EPSP) or when synapses are stimulated directly by glutamate uncaging in control conditions (UEP) or in the presence of TTX and the VSCC cocktail (T+C).

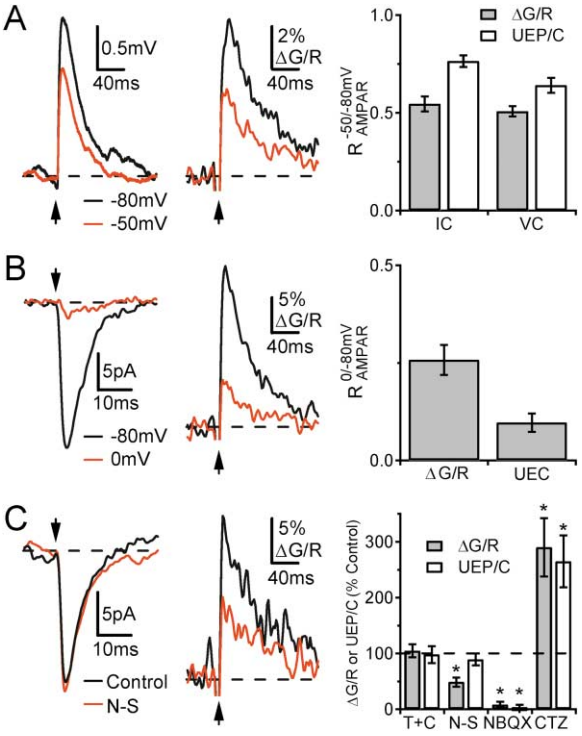

Figure 4. Ca-Permeable AMPARs Contribute to Spine Ca Signals and Are Regulated by Subthreshold Depolarization

(A) AMPAR-mediated UEPs (left) and spine fluorescence transients (middle), at −80 mV (black) and −50 mV (red), with CPP present. Right: Summary of the effects of depolarization to −50 mV on AMPAR-mediated spine $\Delta G/R_{syn}$ and synaptic responses (UEP/C), in current-clamp recordings (IC) and in voltage-clamp recordings (VC) with TTX and VSCC blockers present.

(B) AMPAR-mediated UECs (left) and spine fluorescence transients (middle), at −80 mV (black) and 0 mV (red). Right: Summary of the effects of depolarization to 0 mV on AMPAR-mediated spine $\Delta G/R_{syn}$ and UECs.

(C) Local application of NHPP-spermine (N-S) has little effect on the AMPAR-mediated UEC at −80 mV (left) but reduces the spine fluorescence transients (middle). Right: Summary of the block of AMPAR-mediated spine $\Delta G/R_{syn}$ and synaptic responses (UEP/C) at −80 mV due to local application of TTX and the VSCC cocktail (T+C), N-S, NBQX, or cyclothiazide (CTZ). Asterisk indicates significant difference from 100%.

ductances affect the UEP amplitude and time course recorded at the soma, they are not required for the effects of upstate transitions on local $\Delta[Ca]_{syn}$, which may instead reflect direct regulation of Ca influx through AMPARs and NMDARs.

Ca-Permeable AMPARs Mediate Fast Synaptic Ca Signals in Spines

The fast rise of $\Delta[Ca]_{syn}$ seen in Figure 3 suggested that AMPARs might contribute to this response. Uncaging-evoked AMPAR-mediated $\Delta[Ca]_{syn}$ was revealed in MSNs when NMDARs were blocked with CPP (10 μM) (Figure 4). In current clamp recordings, AMPAR-mediated $\Delta G/R_{syn}$ at −80 mV rose and decayed quickly (Figure 4A), with smaller amplitude than $\Delta G/R_{bAP}$ (5.0% ± 0.5% versus 8.3% ± 0.5%; measured with 100 μM Fluo-4) but similar decay (69 ± 8 ms versus 66 ± 11 ms). Subthreshold depolarization reduced the amplitude of both AMPAR-mediated $\Delta[Ca]_{syn}$ and UEPs ($R^{-50/-80mV}_{\Delta G/R,AMPAR}$ was 0.54 ± 0.05; $R^{-50/-80mV}_{UEP,AMPAR}$ was 0.76 ± 0.04; n = 8 cells, 13 spines) (Figure 4A). One concern was that postsynaptic receptors activated by 2PLU might be different from those activated by presynaptic release. However, we found that electrical stimulation could also evoke AMPAR-mediated $\Delta[Ca]_{syn}$ and EPSPs and that subthreshold depolarization reduced their amplitudes to a similar extent (n = 6 cells, 6 spines; Supplemental Figure S2A).

AMPAR-mediated $\Delta[Ca]_{syn}$ could arise from Ca influx through VSCCs opened by the UEP (Miyakawa et al., 1992; Denk et al., 1995; Reid et al., 2001). However, local application of TTX and the VSCC cocktail had no effect on AMPAR-mediated $\Delta G/R_{syn}$ (105% ± 12% of control) or UEPs (98% ± 15% of control) at −80 mV (n = 5 cells, 6 spines). Moreover, in voltage-clamp recordings with TTX and the VSCC cocktail in the bath, AMPAR-mediated $\Delta[Ca]_{syn}$ was still present and the effect of depolarization was the same ($R^{-50/-80mV}_{\Delta G/R,AMPAR}$ was 0.51 ± 0.03; $R^{-50/-80mV}_{UEC,AMPAR}$ was 0.65 ± 0.04; n = 5 cells, 9 spines) (Figure 4A). These results suggest that AMPAR-mediated $\Delta[Ca]_{syn}$ is not due to VSCC activation and instead reflects direct Ca influx through activated receptors.

Ca-permeable AMPARs have been described in aspiny interneurons (Goldberg et al., 2003) and Purkinje cells (Denk et al., 1995). Both GluR1 and GluR2 subunits have been identified in MSN spines, but whether Ca-permeable AMPARs assemble is unknown. We performed two types of experiments to test for Ca-permeable AMPARs in MSN spines while in the presence of CPP, TTX, and the VSCC cocktail. First, holding at 0 mV to both inactivate any VSCC resistant to the cocktail and minimize the UEC to eliminate voltage-clamp errors, AMPAR-mediated $\Delta[Ca]_{syn}$ was still present ($R^{0/-80mV}_{\Delta G/R,AMPAR}$ was 0.26 ± 0.04; $R^{0/-80mV}_{UEC,AMPAR}$ was 0.10 ± 0.02; n = 7 cells, 8 spines) (Figure 4B). Second, local application of the Ca-permeable AMPAR blocker NHPP-Spermine (50 μM) at −80 mV significantly reduced AMPAR-mediated $\Delta G/R_{syn}$ but not UECs (n = 4 cells, 5 spines) (Figure 4C). In contrast, NBQX (10 μM; n = 4 cells, 5 spines) abolished and cyclothiazide (40 μM; n = 4 cells, 5 spines) greatly enhanced both AMPAR-mediated $\Delta G/R_{syn}$ and UECs (Figure 4C). Thus, these two approaches indicate that direct Ca influx through AMPARs provides a source of Ca into MSN spines.

NMDARs Mediate Slow Synaptic Ca Signals in Spines

The large increase in $\Delta[Ca]_{syn}$ seen with subthreshold depolarization may be explained by enhanced NMDAR-mediated Ca influx. NMDAR-mediated Ca signals are particularly important for induction of synaptic plasticity in MSNs (Calabresi et al., 1992; Partridge et al., 2000). Uncaging-evoked NMDAR-mediated $\Delta[Ca]_{syn}$ was isolated by blocking AMPARs with NBQX (10 μM) and including TTX and the VSCC cocktail in the bath (Figure 5A). Laser power and uncaging pulse duration parameters were similar to those for AMPAR experiments, but adjusted to maintain $\Delta G/R_{syn}$ within the linear range of the Ca indicator. NMDAR-mediated $\Delta G/R_{syn}$ had slower rising and decay phases than $\Delta G/R_{bAP}$, consistent with

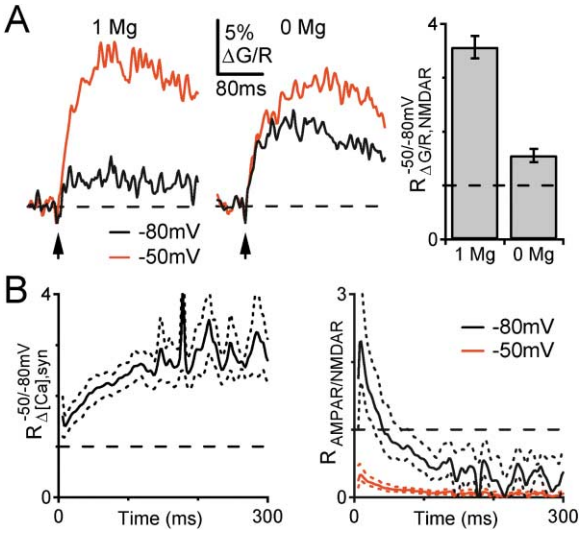

Figure 5. Subthreshold Depolarization Directly Gates Ca Influx through NMDARs

(A) NMDAR-mediated spine fluorescence transients evoked by glutamate uncaging in 1 mM (left) and 0 mM (middle) Mg at −80 mV (black) and −50 mV (red) in voltage-clamp recordings with NBQX, TTX, and VSCC blockers present. Right: Summary of the effects of depolarization to −50 mV on NMDAR-mediated spine $\Delta G/R_{syn}$ in 1 mM or 0 mM Mg.

(B) Left: Ratio of uncaging-evoked spine $\Delta[Ca]_{syn}$ at −50 mV and −80 mV, with both AMPARs and NMDARs available and with TTX and VSCC blockers present. Right: Ratio of AMPAR to NMDAR contributions to the spine $\Delta[Ca]_{syn}$ at −80 mV (black) and −50 mV (red). Solid lines are the means and dotted lines are ±SEM.

prolonged opening of NMDARs following glutamate binding and similar to previous results in pyramidal neurons (Koester and Sakmann, 1998; Kovalchuk et al., 2000; Mainen et al., 1999; Sabatini et al., 2002). On average, subthreshold depolarization greatly increased NMDAR-mediated $\Delta[Ca]_{syn}$ ($R^{-50/-80mV}_{\Delta G/R,NMDAR}$ was 3.6 ± 0.2; n = 7 cells, 18 spines) (Figure 5A). However, this influence was substantially reduced in experiments in which external magnesium (Mg) was removed ($R^{-50/-80mV}_{\Delta G/R,NMDAR}$ was 1.6 ± 0.1; n = 6 cells, 12 spines) (Figure 5A). Thus, subthreshold depolarization provides partial relief of Mg block of the NMDAR and greatly increases Ca influx through the receptor. Local application of 10 μM CPP abolished NMDAR-mediated $\Delta G/R_{syn}$ at −50 mV (1% ± 1% of control; n = 4 cells, 6 spines). Last, we also found that electrical stimulation could evoke NMDAR-mediated $\Delta[Ca]_{syn}$ and EPSCs in the absence of TTX and the VSCC cocktail and that subthreshold depolarization increased their amplitudes to a similar extent (n = 6 cells, 7 spines; Supplemental Figure S2B).

State Transitions Shift AMPAR and NMDAR Contributions

These results indicate that upstate transitions decrease $\Delta[Ca]_{syn}$ mediated by AMPARs while increasing that mediated by NMDARs. Which glutamate receptor contributes the majority of Ca influx in the down- and upstates? To answer this question, we exploited the differential sensitivity of each receptor class to membrane potential to calculate their relative contributions to total $\Delta[Ca]_{syn}$ (see Experimental Procedures). We found that, in the presence of TTX and VSCC blockers, $R^{-50/-80mV}_{\Delta[Ca],syn}$ was 1.5 ± 0.2 in the first 10 ms following stimulation but had risen to 2.9 ± 0.5 by 200 ms (n = 4 cells, 8 spines) (Figure 5B). These values are intermediate to those expected for AMPAR-only and NMDAR-only mediated Ca influx (0.5 and 3.6, respectively), indicating mixed Ca sources at both time points. $R^{-50/-80mV}_{\Delta[Ca],syn}$ is determined by the relative contribution of Ca influx through each receptor subtype and can be used to calculate the ratio of Ca influx through AMPARs to that through NMDARs ($R_{AMPAR/NMDAR}$) (see Experimental Procedures). Thus, at −80 mV, $R^{-80mV}_{AMPAR/NMDAR}$ was 2.4 ± 0.6 at 10 ms and 0.4 ± 0.2 by 200 ms (Figure 5B), indicating that AMPARs dominate the early phase of Ca influx but NMDARs contribute to the late phase. In contrast, at −50 mV, $R^{-50mV}_{AMPAR/NMDAR}$ was 0.3 ± 0.1 at 10 ms and 0.02 ± 0.03 by 200 ms (Figure 5B), indicating that NMDARs dominate both the early and late phases.

bAP Pairing Further Enhances NMDAR Ca Influx in the Upstate

Our results indicate that subthreshold depolarization can profoundly alter the sources and kinetics of Ca signals in spines. In vivo, transitions to the upstate are also characterized by MSNs firing bursts of APs (Stern et al., 1998; Wilson and Kawaguchi, 1996). Nonlinear interactions between bAPs and synaptic inputs influence Ca signals in dendrites and spines of other principal neurons and can trigger the induction of synaptic plasticity (Magee and Johnston, 1997; Markram et al., 1997). We therefore examined whether pairing bAPs with NMDAR activation was able to further increase spine Ca signals beyond that due to subthreshold depolarization (Figure 6).

We found that, at −50 mV and in the presence of NBQX, pairing a single UEP with a bAP delayed by 20 ms resulted in a spine Ca signal larger than expected from the sum of the Ca signals evoked by the UEP and bAP alone (Figure 6A). We quantified this nonlinear enhancement as a percent increase ("boosting") of the NMDAR-mediated Ca signal evoked by the UEP (see Experimental Procedures). On average, in control conditions, pairing led to a significant boosting of 48% ± 6% (n = 5 cells, 8 spines). Is this increase due to increased Ca influx through NMDARs or does NMDAR activation reciprocally influence bAP-evoked Ca entry through VSCC? In the presence of the VSCC cocktail (Figure 6A), $\Delta G/R_{bAP}$ was abolished but pairing resulted in a boosting similar to that seen in control conditions (n = 4 cells, 7 spines). In contrast, when external Mg was removed (Figure 6A), $\Delta G/R_{bAP}$ was present but no boosting occurred (n = 3 cells, 5 spines). These results demonstrate that pairing-induced nonlinearities in Ca influx do not require VSCC activation, and instead reflect increased Ca influx through NMDARs due to further relief of Mg block.

Finally, we asked whether the bursts of bAPs that occur in vivo could further increase spine Ca signals above that due to a single bAP (Figure 6B). At −50 mV and in the presence of NBQX and the VSCC cocktail, the fluorescence transient evoked by a burst of 5 bAPs at 50 Hz was abolished. However, pairing a single UEP

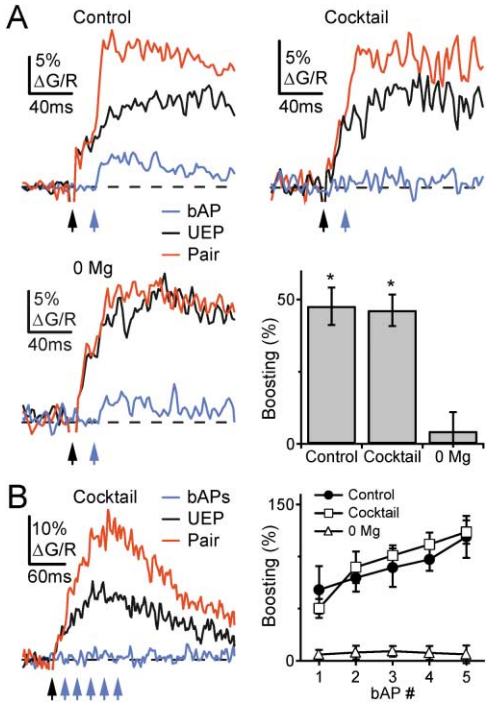

Figure 6. Pairing of bAPs with Synaptic Stimulation Boosts NMDAR-Mediated Spine Ca Signals

(A) Spine fluorescence transients due to bAP alone (blue), UEP alone (black), and UEP paired with bAP (red). Recordings were made in control conditions with 1 mM Mg (top left), in 1 mM Mg with the VSCC cocktail present (top right), or in 0 mM Mg (bottom left). Bottom right: Summary of NMDAR-mediated Ca signal boosting due to bAP pairing in the three conditions. Asterisk indicates significant difference from zero.

(B) Left: Spine fluorescence transients in 1 mM Mg and the VSCC cocktail, evoked by a burst of 5 bAPs at 50 Hz (blue), UEP (black), and UEP paired with the bAPs (red). Right: Summary of boosting of NMDAR-mediated Ca signal due to pairing, for 20 ms following each bAP in the burst, in control conditions, in the presence of the VSCC cocktail, and in 0 mM Mg.

In (A) and (B), blue and black arrows indicate the timing of bAPs and UEP, respectively.

with the burst led to additional boosting of the NMDAR-mediated Ca signal by each bAP in the train. Thus, boosting was 120% ± 10% following the last bAP, in contrast to 50% ± 9% following the first bAP (n = 4 cells, 8 spines). Similar results were found in control conditions (n = 6 cells, 6 spines), but no boosting was present when external Mg was removed (n = 5 cells, 8 spines). Thus, both isolated bAPs and bursts of bAPs can strongly impact spine Ca signals by increasing Ca influx through activated NMDARs.

Discussion

We have presented a mechanistic analysis of how sub- and suprathreshold depolarizations alter the sources and kinetics of Ca signals within dendrites and spines of MSNs. Our results indicate that state transitions alter evoked Ca signals both by influencing the availability of active conductances and by regulating Ca influx through ionotropic glutamate receptors.

Synaptic Ca Signals in MSNs

We found that synaptic Ca signals in MSNs are restricted to activated spines. Subthreshold depolarization changes both the amplitude and kinetics of $\Delta[Ca]_{syn}$. By combining 2PLSM and 2PLU of glutamate, we could mimic synaptic inputs and monitor $\Delta[Ca]_{syn}$ without electrical stimulation. This technique allowed us to assess the role of active conductances in shaping $\Delta[Ca]_{syn}$ by using selective antagonists that would otherwise block glutamate release. We found that voltage-sensitive Na and Ca conductances are not necessary for the effects of state transitions on $\Delta[Ca]_{syn}$. Instead, these effects are due to changes in Ca influx via Ca-permeable AMPARs and NMDARs.

Ca-Permeable AMPARs in Spines

We found a prominent AMPAR-mediated $\Delta[Ca]_{syn}$ in MSN spines, with similar amplitude and time course to $\Delta[Ca]_{bAP}$. Previous studies demonstrate AMPAR-evoked $\Delta[Ca]_{syn}$ via Ca-permeable AMPARs in aspiny interneurons (Goldberg et al., 2003) and Purkinje cells (Denk et al., 1995) and via VSCCs in hippocampal pyramidal neurons (Miyakawa et al., 1992; Reid et al., 2001) and Purkinje cells (Denk et al., 1995). In MSNs, the AMPAR-mediated $\Delta[Ca]_{syn}$ is via Ca-permeable AMPARs and does not require VSCCs. Subthreshold depolarization decreases this $\Delta[Ca]_{syn}$, likely by reducing the driving force for Ca influx through these receptors. MSNs express both GluR1 and GluR2 and both of these AMPAR subunits can be found in spines (Bernard et al., 1997; Chen et al., 1998; Stefani et al., 1998). The molecular makeup of functional Ca-permeable AMPARs in MSNs remains unknown and may include AMPARs with GluR1 alone and mixed with GluR2. While Ca permeability is usually associated with a lack of GluR2, previous studies have shown that other neurons expressing GluR2 can also have functional Ca-permeable AMPARs (Toth and McBain, 1998). However, the relatively small influence of NHPP-spermine on the AMPAR-mediated UEC suggests that Ca-permeable AMPARs likely comprise only a small fraction of the total AMPAR population in MSN spines.

NMDARs in Spines and Relief of Mg Block

Our results indicate that Ca influx through NMDARs also contributes to $\Delta[Ca]_{syn}$ in MSN spines. Subthreshold depolarization causes a large increase in NMDAR-mediated $\Delta[Ca]_{syn}$, due to relief of Mg block of NMDARs. Heterologous expression studies indicate that Mg block changes approximately 10-fold in the subthreshold range traversed during state transitions (Jahr and Stevens, 1990; Mayer et al., 1984; Nowak et al., 1984). The remaining sensitivity to subthreshold depolarization seen in our experiments in 0 mM Mg is most likely due to residual Mg in the extracellular solution.

We found that single bAPs and bursts lead to boosting of NMDAR-mediated $\Delta[Ca]_{syn}$ in MSN spines. In other central neurons, pairing bAPs with synaptic inputs also can generate Ca signals larger than the sum of the signals evoked by bAPs and synaptic inputs alone (Koester and Sakmann, 1998; Magee and Johnston, 1997; Nevian and Sakmann, 2004; Schiller et al., 1998; Waters et al., 2003; Yuste and Denk, 1995). Recent results in cortical

neurons indicate that boosting in spines is likely due to relief of Mg block of NMDARs (Nevian and Sakmann, 2004). However, boosting could also involve VSCC activation, and these channels cannot be blocked when using extracellular stimulation. We found that boosting in MSN spines is purely via relief of Mg block and does not require VSCCs.

Voltage-Sensitive Ca Channels in Dendrites and Spines

Previous results using somatic recordings identified multiple classes of VSCCs in MSNs (Bargas et al., 1994; Hoehn et al., 1993), but their contributions to Ca signaling in dendrites and spines was unknown. We found that T-, R-, and L-type channels located in dendritic shafts and spine heads mediate $\Delta[Ca]_{bAP}$. In contrast, while N/P/Q-type channels are present in the soma (Bargas et al., 1994; Hoehn et al., 1993), they are not activated by single bAPs in dendrites and spines.

T-type channels contribute to evoked Ca signals in dendrites of hippocampal pyramidal neurons (Magee et al., 1995) and spines of granule cells in the olfactory bulb (Egger et al., 2003). In MSNs, Ni^{2+}-sensitive Ca influx comprises more than 50% of $\Delta[Ca]_{bAP}$ at −80 mV. Multiple classes of T-type VSCCs expressed in striatum, including $Ca_v3.1$, $Ca_v3.2$, and $Ca_v3.3$ (McRory et al., 2001), could mediate this Ca influx, although some R-type channels are also sensitive to this concentration of Ni^{2+} (Foehring et al., 2000). The Ni^{2+}-sensitive component of $\Delta[Ca]_{bAP}$ is greatly reduced at −50 mV, possibly reflecting inactivation of T-type channels at this potential (Hoehn et al., 1993). Interestingly, $Ca_v3.3$ channels are selectively expressed in the striatum and have negatively shifted activation and inactivation curves that may make them selectively available near −80 mV (McRory et al., 2001).

$\Delta[Ca]_{bAP}$ in dendrites and spines of hippocampal pyramidal neurons is thought to be mediated by R-type channels due to insensitivity to other VSCC blockers (Sabatini and Svoboda, 2000; Yasuda et al., 2003). We found that SNX-482-sensitive Ca influx contributes approximately 40% of $\Delta[Ca]_{bAP}$ at both −80 mV and −50 mV. This Ca influx is likely via R-type channels comprised of $Ca_v2.3$ subunits expressed in MSNs (Foehring et al., 2000). The similar block at the two potentials suggests that these channels do not significantly inactivate at −50 mV in a physiological setting.

L-type channels play a role in generating somatic Ca signals and modulating both AP firing and EPSP amplitude in MSNs (Akopian and Walsh, 2002; Cepeda et al., 1998; Hernandez-Lopez et al., 1997). We found that nimodipine-sensitive Ca influx makes a significant contribution to $\Delta[Ca]_{bAP}$ at −50 mV. This Ca influx could be due to multiple classes of L-type channels found in MSNs (Song and Surmeier, 1996). While all of these channels should be blocked by the relatively high concentration of nimodipine used, $Ca_v1.3$ channels may be less sensitive (50% block) at hyperpolarized potentials (Xu and Lipscombe, 2001). However, it is unlikely that these channels contribute to $\Delta[Ca]_{bAP}$ at −80 mV, since Ni^{2+} and SNX-482 block approximately 90% of this signal. Lastly, our results contrast with hippocampal pyramidal neurons, where L-type channels do not significantly contribute to $\Delta[Ca]_{bAP}$ (Sabatini and Svoboda, 2000) despite playing a role in activating downstream Ca-sensitive processes (Yasuda et al., 2003).

Mibefradil is often used to selectively block T-type channels, and we initially used it for this purpose. Mibefradil-sensitive Ca influx contributes 40% of $\Delta[Ca]_{bAP}$ at −80 mV, and significantly more at −50 mV. However, mibefradil can also block certain classes of R- and L-type channels in a voltage-dependent manner (Jimenez et al., 2000), rendering the interpretation of the differential effects of mibefradil at −80 mV and −50 mV difficult. Although how mibefradil blocks $\Delta[Ca]_{bAP}$ remains undefined, it was useful for our experiments in which Ca influx through VSCCs needed to be eliminated. Thus, the VSCC cocktail consisting of mibefradil, SNX-482, ω-conotoxin-MVIIC, and nimodipine completely blocks Ca signals evoked by both single bAPs and bursts.

State Transitions Influence Spine Ca Signals

We found that state transitions alter not only the sources, but also the amplitude and kinetics of spine Ca signals. Given our estimate of K_E and the rapid decay time constant for $\Delta[Ca]_{bAP}$, [Ca] within spine heads of unperturbed MSNs responds quickly to Ca influx. The time course of AMPAR-mediated $\Delta[Ca]_{syn}$ is similar to $\Delta[Ca]_{bAP}$, due to rapid receptor kinetics, while the time course of NMDAR-mediated $\Delta[Ca]_{syn}$ is slower, due to prolonged receptor opening. In the downstate, AMPAR activation generates a large Ca signal that initially dominates but gradually overlaps with the smaller Ca signal due to NMDAR activation. In the upstate, Ca influx via NMDARs dominates throughout, so that the total $\Delta[Ca]_{syn}$ gradually builds and decays. Since bAP duration is brief and Mg rebinding to NMDARs is rapid, boosting by bAPs results in only a short-lived additional NMDAR-mediated Ca signal. The continued boosting by each bAP in a burst is likely via sequential relief of Mg block during the long time course of NMDAR activation. However, summation of this boosting is unlikely to occur in vivo for bAP frequencies <50 Hz, due to faster Ca clearance in the absence of exogenous Ca buffers.

In vivo, state transitions in MSNs are driven by synaptic inputs from the cortex and thalamus (Wilson and Kawaguchi, 1996). In acute slices or dissociated MSNs, spontaneous state transitions do not occur and are instead usually mimicked with somatic depolarization (Hernandez-Lopez et al., 1997). In long-term corticostriatal cultures, spontaneous upstates occur that are driven by concerted synaptic inputs (Plenz and Kitai, 1998). Dendritic Ca signals occur during upstates (Kerr and Plenz, 2002) and are boosted by suprathreshold activity with bAPs occurring soon after the upstate transition, generating larger increases than those occurring later (Kerr and Plenz, 2004). However, how relief of Mg block contributes to this boosting is difficult to determine, because 0 mM extracellular Mg perturbs the slice network that generates the upstates.

Functional Ca Signals

As in many other neurons, NMDAR activation is important for synaptic plasticity in MSNs (Calabresi et al., 1992; Partridge et al., 2000). Inducing NMDAR-dependent long-term potentiation (LTP) is notoriously difficult

in MSNs, usually requiring unphysiologically low extracellular Mg concentrations (Calabresi et al., 1992; Partridge et al., 2000). However, analysis of LTP has been limited to MSNs in the downstate, where NMDAR-mediated $\Delta[Ca]_{syn}$ is reduced and AMPAR-mediated $\Delta[Ca]_{syn}$ is considerable. We speculate that triggering NMDAR-dependent LTP may be greatly facilitated by upstate transitions, where NMDAR-mediated $\Delta[Ca]_{syn}$ is enhanced. Moreover, bAP boosting of NMDAR-mediated $\Delta[Ca]_{syn}$ during the upstate may allow spike-timing dependent plasticity similar to that observed in other principal neurons.

Multiple downstream signaling pathways are sensitive to the source and location of Ca signals. In hippocampal neurons, Ca signals via L-type channels (Yasuda et al., 2003) and NMDARs (Silva et al., 1992) can activate CaM KII. In MSNs, activation of NMDARs can ultimately lead to dephosphorylation of DARPP-32 (Halpain et al., 1990; Nishi et al., 2002), an important target of dopamine receptor signaling. Moreover, activation of both L-type channels (Liu and Graybiel, 1996; Rajadhyaksha et al., 1999) and NMDARs (Konradi et al., 1996) can trigger CREB phosphorylation and induce immediate early gene expression. By allowing different Ca sources to be activated, state transitions may determine which downstream signaling pathways are triggered in response to synaptic activity. Thus, we find that state transitions not only serve to gate the output of striatum, but also regulate physiological and intracellular responses to glutamatergic input. Finally, our results likely apply to other classes of principal neurons that also exhibit state transitions in vivo (Lampl et al., 1999; Steriade et al., 1993).

Experimental Procedures

Electrophysiology

Coronal slices (300 μm thick) were cut from the dorsal striatum of 15- to 19-day-old Sprague Dawley rats in ice-cold external solution containing (in mM): 110 choline, 25 $NaHCO_3$, 1.25 NaH_2PO_4, 2.5 KCl, 7 $MgCl_2$, 0.5 $CaCl_2$, 25 glucose, 11.6 Na-ascorbate, and 3.1 Na-pyruvate, bubbled with 95% O_2/5% CO_2. Slices were transferred to ACSF containing (in mM): 127 NaCl, 25 $NaHCO_3$, 1.25 NaH_2PO_4, 2.5 KCl, 1 $MgCl_2$, 2 $CaCl_2$, and 25 glucose, bubbled with 95% O_2/5% CO_2. After 40 min at 34°C, slices were stored at 24°C, and experiments were conducted at 30°C–32°C. In all experiments, 10 μM bicuculline was present in the ACSF. In all experiments examining synaptic responses, 100 μM LY-341495 was present in the ACSF to block mGluRs. In experiments examining NMDAR-mediated synaptic responses, 10 μM serine was added to the ACSF. In some experiments, one or more of the following drugs were added to the ACSF or locally applied using pressure ejection from a nearby micropipette (in μM): 10 NBQX, 10 CPP, 1 TTX, 50 $NiCl_2$, 0.3 SNX-482, 1 ω-conotoxin-MVIIC, 20 nimodipine, 20 mibefradil, 50 NHPP-spermine, and 40 cyclothiazide. For uncaging experiments, 2.5 or 5 mM MNI-glutamate (Tocris) was also added to the ACSF.

Whole-cell recordings were obtained from MSNs identified with video-IRDIC. MSNs represent the major cell type in the striatum, have small cell bodies, and are the only neurons with prominent dendritic spines. Glass electrodes (3–5 MΩ) were filled with 1 of 2 internal solutions. Whole-cell current-clamp recordings used solution 1 (in mM): 135 $KMeSO_3$, 10 HEPES, 4 $MgCl_2$, 4 Na_2ATP, 0.4 NaGTP, and 10 $Na_2CreatinePO_4$ (pH 7.4) with KOH. Whole-cell voltage-clamp recordings used solution 2 (in mM): 135 $CsMeSO_3$, 10 HEPES, 4 $MgCl_2$, 4 Na_2ATP, 0.4 NaGTP, and 10 $Na_2CreatinePO_4$ (pH 7.4) with CsOH. Electrodes also contained either 100 μM Fluo-4 or 300 μM Fluo-5F to monitor calcium levels and 10 μM Alexa Fluor-594 to image the neuronal morphology. Fluo-4 was used for recording bAP- and some AMPAR-mediated Ca signals, and Fluo-5F was used for recording total synaptic-NMDAR, and the remaining AMPAR-mediated Ca signals.

Imaging

Uncaging of MNI-glutamate and intracellular Ca imaging was accomplished with a custom built microscope combining 2PLSM and 2PLU. The outputs of 2 Ti:Sapphire lasers (Mira/Verdi, Coherent, Santa Clara, CA) were independently modulated with Pockel's cells (350-80 and 350-50, Conoptics, Danbury, CT) and gated with mechanical shutters (VS25S2ZM1 and LS6Z2, Uniblitz, Vincent Associates, Rochester, NY). One laser was tuned to 720 nm for photoactivation of MNI-glutamate and its polarization was rotated 90° (PBSH-670-980-050 and MWPS-830-05-2-B, CVI Laser, Albuquerque, NM). The second was tuned to 810 nm for excitation of Alexa Fluor-594 and either Fluo-4 or Fluo-5F. The laser outputs were combined using a second polarizing beam splitter and directed to scanning galvanometers (6210, Cambridge Technology, Cambridge, MA). The scanning mirrors were focused onto the back focal plane of the objective (63×, 0.9 NA, Olympus, Melville, NY) with a scan lens (Olympus) and tube lens (CVI laser) (Yasuda et al., 2003). Shortpass dichroics (700DCXR) and interference filters (E700SP-2P) were used to eliminate excitation laser light. Emitted photons were collected in epifluorescence and transfluorescence (oil-immersion condenser, NA = 1.4, Olympus) modes using photomultiplier tubes (R3896, Hamamatsu, Hamamatsu City, Japan). "Green" and "red" emitted photons were separated using a dichroic (565DCXR), green colored glass (BG22), and a barrier filter (607/45). All filters and dichroics were from Chroma (Battleboro, VT).

Neurons were filled via the patch electrode for 10–20 min before imaging. Red fluorescence was used to locate dendritic spines 30–75 μm from the soma. To measure Ca signals, green and red fluorescence was collected during 500 Hz line scans across the spine head and parent dendrite. Offsets from the photomultiplier and preamplifier were measured in the dark and subtracted from the measurement. No further background correction was performed, as autofluorescence is negligible in 2PLSM. Fluorescence changes were quantified as increases in green fluorescence from baseline normalized to the red fluorescence ($\Delta G/R$) (Sabatini et al., 2002). For Fluo-4 and Fluo-5F, we measured $\Delta G/R_{max}$ at saturation (0.55 and 1.6) and $\Delta G/R_{rest}$ at rest (0.05 and 0.1) for our microscope. During experiments, $\Delta G/R$ signals (<0.1 and 0.3) were <20% of ($\Delta G/R_{max} - \Delta G/R_{rest}$), giving a linearity error of <20%. Back-propagating action potentials were induced by somatic current injection (2–6 nA, 5 ms). Excitatory input fibers were stimulated with a small glass electrode (tip diameter 2–4 μm) filled with ACSF placed 10–50 μm from the spine of interest, with brief (0.2 ms) and small (10–20 μA) current injections. Glutamate was uncaged using 0.2–0.5 ms pulses gated by the Pockel's cell while the scanning mirrors were temporarily (1–2 ms) redirected to the spine of interest. To ensure that uncaging was performed in a constant location, image drift was corrected automatically before each line scan acquisition by collecting a frame scan and calculating the cross-correlation to a reference image. Adjustment of the scan angles of the galvanometers was used to negate the calculated drift.

Data Acquisition and Analysis

Image acquisition was performed using ScanImage software (Pologruto et al., 2003). Physiology acquisition, Pockel's cell control, image drift correction, and online data analysis was performed using custom software written in Matlab (Mathworks). Offline data analysis was performed using custom software written in Igor Pro (Wavemetrics). $\Delta G/R$ amplitude values for bAP- and AMPAR-mediated transients are averages over a 20 ms time period, those for total synaptic- and NMDA-mediated transients are averages over a 150 ms time period, and those for pairing experiments are averages over a 20 ms time period. $\Delta G/R$ decay values are taus from single exponential fits. Peak EPSP/UEP and EPSC/UEC values are averages of a 1 ms time period surrounding the maximum absolute amplitude, and decays are half-decay times. Summary data are reported as mean ± SEM. Significance was defined as $p < 0.05$, using the two-tailed Student's t test.

Calculation of the AMPAR to NMDAR Ratio

For the analysis of the relative contribution of AMPARs and NMDARs to the $\Delta[Ca]_{syn}$ (Figure 5), the following rationale was used. First, we assumed linearity of the Ca indicator and linear summation of Ca signals. Second, we define $R^{-50/-80mV}_{\Delta[Ca],syn}$ as the ratio of the synaptic Ca signals at −50 mV to that at −80 mV in conditions with AMPARs and NMDARs active but Na and Ca channels blocked:

$$R^{-50/-80mV}_{\Delta[Ca],syn} = \frac{\Delta[Ca]^{-50mV}_{syn}}{\Delta[Ca]^{-80mV}_{syn}} = \frac{\Delta G/R^{-50mV}_{syn}}{\Delta G/R^{-80mV}_{syn}}$$

$$= \frac{\Delta G/R^{-50mV}_{AMPAR} + \Delta G/R^{-50mV}_{NMDAR}}{\Delta G/R^{-80mV}_{AMPAR} + \Delta G/R^{-80mV}_{NMDAR}}$$

$$= \frac{0.5\Delta G/R^{-80mV}_{AMPAR} + 3.5\Delta G/R^{-80mV}_{NMDAR}}{\Delta G/R^{-80mV}_{AMPAR} + \Delta G/R^{-80mV}_{NMDAR}}$$

(using results of Figures 4A and 5A). From which one can solve

$$R^{-80mV}_{AMPAR/NMDAR} = \frac{\Delta G/R^{-80mV}_{AMPAR}}{\Delta G/R^{-80mV}_{NMDAR}} = \frac{R^{-50/-80mV}_{\Delta[Ca],syn} - 3.5}{0.5 - R^{-50/-80mV}_{\Delta[Ca],syn}} \text{ and}$$

$$R^{-50mV}_{AMPAR/NMDAR} = \frac{\Delta G/R^{-50mV}_{AMPAR}}{\Delta G/R^{-50mV}_{NMDAR}} = \frac{R^{-50/-80mV}_{\Delta[Ca],syn}/3.5 - 1}{1 - 2(R^{-50/-80mV}_{\Delta[Ca],syn})}.$$

Calculation of NMDAR Boosting

For the analysis of changes in NMDAR-mediated Ca signal due to pairing with bAPs (Figure 6), we conceptualized the pairing-evoked Ca signal as the sum of the signals evoked by the UEP alone, the bAP alone, and a term that describes the extra Ca influx due to nonlinear interactions between the UEP and bAP:

$$\Delta[Ca]_{pair} = \Delta[Ca]_{UEP} + \Delta[Ca]_{bAP} + \Delta[Ca]_{nonlinear}.$$

Expressing the amplitude of the nonlinear term as a percentage of the UEP-evoked Ca signal, which we refer to as the boosting, we get:

$$boosting = 100\left(\frac{\Delta[Ca]_{nonlinear}}{\Delta[Ca]_{UEP}}\right) = 100\left(\frac{\Delta[Ca]_{pair} - \Delta[Ca]_{UEP} - \Delta[Ca]_{bAP}}{\Delta[Ca]_{UEP}}\right)$$

$$= 100\left(\frac{\Delta G/R_{pair} - \Delta G/R_{bAP}}{\Delta G/R_{UEP}} - 1\right).$$

Buffer Capacity Measurement

The Ca buffer capacity (K) is approximately the ratio of the number of bound Ca ions to free Ca ions for a given Ca influx. We measured the differential Ca buffer capacity (K_E) by competing endogenous buffers with increasing concentrations of exogenous buffers (20 [n = 8], 50 [n = 10], 100 [n = 7], and 200 [n = 8] μM Fluo-4) (Helmchen et al., 1996; Maravall et al., 2000; Sabatini et al., 2002). $\Delta G/R_{bAP}$ was converted to $\Delta[Ca]_{bAP}$ as described previously using the maximum fluorescence at indicator saturation (Maravall et al., 2000; Sabatini et al., 2002). Plotting the inverse peak $\Delta[Ca]_{bAP}$ against the exogenous buffer capacity (K_B) reveals a linear relationship for both spines and dendrites. K_E is given by the x-intercept of this plot and measures 84 (range 62–137) in spines and 96 (range 38–146) in dendrites. The amplitude of $\Delta[Ca]_{bAP}$ in conditions of zero added buffer is given by the y axis intercept and is ∼400 nM. In 100 μM Fluo-4, K_B is ∼180 and the τ_{decay} for $\Delta[Ca]_{bAP}$ is ∼70 ms. Thus, we estimate the τ_{decay} for $\Delta[Ca]_{bAP}$ in conditions of zero added buffer to be ∼25 ms. Because Ca influx via VSCCs on this time scale is brief, this represents the kinetics of the impulse response of the spine to changes in [Ca].

Acknowledgments

We thank members of the Sabatini lab, N. Blair, and M. Xu-Freidman for comments on the manuscript. This work was supported by NIH T32 NS07484 (to A.G.C.) and Burroughs Wellcome Fund Career Award, McKnight Technological Innovations Grant, and NINDS (RO1 NS046579-01A) (to B.L.S.). The authors declare that they have no financial conflicts of interests.

Received: July 9, 2004
Revised: September 7, 2004
Accepted: September 24, 2004
Published: October 27, 2004

References

Akopian, G., and Walsh, J.P. (2002). Corticostriatal paired-pulse potentiation produced by voltage-dependent activation of NMDA receptors and L-type Ca(2+) channels. J. Neurophysiol. *87*, 157–165.

Bargas, J., Howe, A., Eberwine, J., Cao, Y., and Surmeier, D.J. (1994). Cellular and molecular characterization of Ca^{2+} currents in acutely isolated, adult rat neostriatal neurons. J. Neurosci. *14*, 6667–6686.

Bernard, V., Somogyi, P., and Bolam, J.P. (1997). Cellular, subcellular, and subsynaptic distribution of AMPA-type glutamate receptor subunits in the neostriatum of the rat. J. Neurosci. *17*, 819–833.

Calabresi, P., Pisani, A., Mercuri, N.B., and Bernardi, G. (1992). Long-term potentiation in the striatum is unmasked by removing the voltage-dependent magnesium block of NMDA receptor channels. Eur. J. Neurosci. *4*, 929–935.

Cepeda, C., Colwell, C.S., Itri, J.N., Chandler, S.H., and Levine, M.S. (1998). Dopaminergic modulation of NMDA-induced whole cell currents in neostriatal neurons in slices: contribution of calcium conductances. J. Neurophysiol. *79*, 82–94.

Chen, Q., Veenman, L., Knopp, K., Yan, Z., Medina, L., Song, W.J., Surmeier, D.J., and Reiner, A. (1998). Evidence for the preferential localization of glutamate receptor-1 subunits of AMPA receptors to the dendritic spines of medium spiny neurons in rat striatum. Neuroscience *83*, 749–761.

Denk, W., Sugimori, M., and Llinas, R. (1995). Two types of calcium response limited to single spines in cerebellar Purkinje cells. Proc. Natl. Acad. Sci. USA *92*, 8279–8282.

Egger, V., Svoboda, K., and Mainen, Z.F. (2003). Mechanisms of lateral inhibition in the olfactory bulb: efficiency and modulation of spike-evoked calcium influx into granule cells. J. Neurosci. *23*, 7551–7558.

Fierro, L., and Llano, I. (1996). High endogenous calcium buffering in Purkinje cells from rat cerebellar slices. J. Physiol. *496*, 617–625.

Foehring, R.C., Mermelstein, P.G., Song, W.J., Ulrich, S., and Surmeier, D.J. (2000). Unique properties of R-type calcium currents in neocortical and neostriatal neurons. J. Neurophysiol. *84*, 2225–2236.

Goldberg, J.H., Tamas, G., Aronov, D., and Yuste, R. (2003). Calcium microdomains in aspiny dendrites. Neuron *40*, 807–821.

Halpain, S., Girault, J.A., and Greengard, P. (1990). Activation of NMDA receptors induces dephosphorylation of DARPP-32 in rat striatal slices. Nature *343*, 369–372.

Helmchen, F., Imoto, K., and Sakmann, B. (1996). Ca^{2+} buffering and action potential-evoked Ca2+ signaling in dendrites of pyramidal neurons. Biophys. J. *70*, 1069–1081.

Hernandez-Lopez, S., Bargas, J., Surmeier, D.J., Reyes, A., and Galarraga, E. (1997). D1 receptor activation enhances evoked discharge in neostriatal medium spiny neurons by modulating an L-type Ca^{2+} conductance. J. Neurosci. *17*, 3334–3342.

Hoehn, K., Watson, T.W., and MacVicar, B.A. (1993). Multiple types of calcium channels in acutely isolated rat neostriatal neurons. J. Neurosci. *13*, 1244–1257.

Jahr, C.E., and Stevens, C.F. (1990). A quantitative description of NMDA receptor-channel kinetic behavior. J. Neurosci. *10*, 1830–1837.

Jimenez, C., Bourinet, E., Leuranguer, V., Richard, S., Snutch, T.P., and Nargeot, J. (2000). Determinants of voltage-dependent inactivation affect Mibefradil block of calcium channels. Neuropharmacology *39*, 1–10.

Kerr, J.N., and Plenz, D. (2002). Dendritic calcium encodes striatal neuron output during up-states. J. Neurosci. *22*, 1499–1512.

Kerr, J.N., and Plenz, D. (2004). Action potential timing determines dendritic calcium during striatal up-states. J. Neurosci. *24*, 877–885.

Koester, H.J., and Sakmann, B. (1998). Calcium dynamics in single

spines during coincident pre- and postsynaptic activity depend on relative timing of back-propagating action potentials and subthreshold excitatory postsynaptic potentials. Proc. Natl. Acad. Sci. USA *95*, 9596–9601.

Konradi, C., Leveque, J.C., and Hyman, S.E. (1996). Amphetamine and dopamine-induced immediate early gene expression in striatal neurons depends on postsynaptic NMDA receptors and calcium. J. Neurosci. *16*, 4231–4239.

Kovalchuk, Y., Eilers, J., Lisman, J., and Konnerth, A. (2000). NMDA receptor-mediated subthreshold Ca(2+) signals in spines of hippocampal neurons. J. Neurosci. *20*, 1791–1799.

Lampl, I., Reichova, I., and Ferster, D. (1999). Synchronous membrane potential fluctuations in neurons of the cat visual cortex. Neuron *22*, 361–374.

Lee, S.H., Rosenmund, C., Schwaller, B., and Neher, E. (2000). Differences in Ca^{2+} buffering properties between excitatory and inhibitory hippocampal neurons from the rat. J. Physiol. *525*, 405–418.

Liu, F.C., and Graybiel, A.M. (1996). Spatiotemporal dynamics of CREB phosphorylation: transient versus sustained phosphorylation in the developing striatum. Neuron *17*, 1133–1144.

Magee, J.C., and Johnston, D. (1997). A synaptically controlled, associative signal for Hebbian plasticity in hippocampal neurons. Science *275*, 209–213.

Magee, J.C., Christofi, G., Miyakawa, H., Christie, B., Lasser-Ross, N., and Johnston, D. (1995). Subthreshold synaptic activation of voltage-gated Ca^{2+} channels mediates a localized Ca^{2+} influx into the dendrites of hippocampal pyramidal neurons. J. Neurophysiol. *74*, 1335–1342.

Mainen, Z.F., Malinow, R., and Svoboda, K. (1999). Synaptic calcium transients in single spines indicate that NMDA receptors are not saturated. Nature *399*, 151–155.

Maravall, M., Mainen, Z.F., Sabatini, B.L., and Svoboda, K. (2000). Estimating intracellular calcium concentrations and buffering without wavelength ratioing. Biophys. J. *78*, 2655–2667.

Markram, H., Lubke, J., Frotscher, M., and Sakmann, B. (1997). Regulation of synaptic efficacy by coincidence of postsynaptic APs and EPSPs. Science *275*, 213–215.

Matsuzaki, M., Ellis-Davies, G.C., Nemoto, T., Miyashita, Y., Iino, M., and Kasai, H. (2001). Dendritic spine geometry is critical for AMPA receptor expression in hippocampal CA1 pyramidal neurons. Nat. Neurosci. *4*, 1086–1092.

Matsuzaki, M., Honkura, N., Ellis-Davies, G.C., and Kasai, H. (2004). Structural basis of long-term potentiation in single dendritic spines. Nature *429*, 761–766.

Mayer, M.L., Westbrook, G.L., and Guthrie, P.B. (1984). Voltage-dependent block by Mg^{2+} of NMDA responses in spinal cord neurones. Nature *309*, 261–263.

McRory, J.E., Santi, C.M., Hamming, K.S., Mezeyova, J., Sutton, K.G., Baillie, D.L., Stea, A., and Snutch, T.P. (2001). Molecular and functional characterization of a family of rat brain T-type calcium channels. J. Biol. Chem. *276*, 3999–4011.

Miyakawa, H., Ross, W.N., Jaffe, D., Callaway, J.C., Lasser-Ross, N., Lisman, J.E., and Johnston, D. (1992). Synaptically activated increases in Ca^{2+} concentration in hippocampal CA1 pyramidal cells are primarily due to voltage-gated Ca^{2+} channels. Neuron *9*, 1163–1173.

Nevian, T., and Sakmann, B. (2004). Single spine Ca^{2+} signals evoked by coincident EPSPs and backpropagating action potentials in spiny stellate cells of layer 4 in the juvenile rat somatosensory barrel cortex. J. Neurosci. *24*, 1689–1699.

Nishi, A., Bibb, J.A., Matsuyama, S., Hamada, M., Higashi, H., Nairn, A.C., and Greengard, P. (2002). Regulation of DARPP-32 dephosphorylation at PKA- and Cdk5-sites by NMDA and AMPA receptors: distinct roles of calcineurin and protein phosphatase-2A. J. Neurochem. *81*, 832–841.

Nowak, L., Bregestovski, P., Ascher, P., Herbet, A., and Prochiantz, A. (1984). Magnesium gates glutamate-activated channels in mouse central neurones. Nature *307*, 462–465.

Partridge, J.G., Tang, K.C., and Lovinger, D.M. (2000). Regional and postnatal heterogeneity of activity-dependent long-term changes in synaptic efficacy in the dorsal striatum. J. Neurophysiol. *84*, 1422–1429.

Plenz, D., and Kitai, S.T. (1998). Up and down states in striatal medium spiny neurons simultaneously recorded with spontaneous activity in fast-spiking interneurons studied in cortex-striatum-substantia nigra organotypic cultures. J. Neurosci. *18*, 266–283.

Pologruto, T.A., Sabatini, B.L., and Svoboda, K. (2003). ScanImage: flexible software for operating laser scanning microscopes. Biomed. Eng. Online *2*, 13.

Rajadhyaksha, A., Barczak, A., Macias, W., Leveque, J.C., Lewis, S.E., and Konradi, C. (1999). L-Type Ca(2+) channels are essential for glutamate-mediated CREB phosphorylation and c-fos gene expression in striatal neurons. J. Neurosci. *19*, 6348–6359.

Reid, C.A., Fabian-Fine, R., and Fine, A. (2001). Postsynaptic calcium transients evoked by activation of individual hippocampal mossy fiber synapses. J. Neurosci. *21*, 2206–2214.

Sabatini, B.L., and Svoboda, K. (2000). Analysis of calcium channels in single spines using optical fluctuation analysis. Nature *408*, 589–593.

Sabatini, B.L., Oertner, T.G., and Svoboda, K. (2002). The life cycle of Ca(2+) ions in dendritic spines. Neuron *33*, 439–452.

Schiller, J., Schiller, Y., and Clapham, D.E. (1998). NMDA receptors amplify calcium influx into dendritic spines during associative pre- and postsynaptic activation. Nat. Neurosci. *1*, 114–118.

Silva, A.J., Stevens, C.F., Tonegawa, S., and Wang, Y. (1992). Deficient hippocampal long-term potentiation in alpha-calcium-calmodulin kinase II mutant mice. Science *257*, 201–206.

Smith, M.A., Ellis-Davies, G.C., and Magee, J.C. (2003). Mechanism of the distance-dependent scaling of Schaffer collateral synapses in rat CA1 pyramidal neurons. J. Physiol. *548*, 245–258.

Song, W.J., and Surmeier, D.J. (1996). Voltage-dependent facilitation of calcium channels in rat neostriatal neurons. J. Neurophysiol. *76*, 2290–2306.

Stefani, A., Chen, Q., Flores-Hernandez, J., Jiao, Y., Reiner, A., and Surmeier, D.J. (1998). Physiological and molecular properties of AMPA/Kainate receptors expressed by striatal medium spiny neurons. Dev. Neurosci. *20*, 242–252.

Steriade, M., Nunez, A., and Amzica, F. (1993). A novel slow (< 1 Hz) oscillation of neocortical neurons in vivo: depolarizing and hyperpolarizing components. J. Neurosci. *13*, 3252–3265.

Stern, E.A., Jaeger, D., and Wilson, C.J. (1998). Membrane potential synchrony of simultaneously recorded striatal spiny neurons in vivo. Nature *394*, 475–478.

Toth, K., and McBain, C.J. (1998). Afferent-specific innervation of two distinct AMPA receptor subtypes on single hippocampal interneurons. Nat. Neurosci. *1*, 572–578.

Vergara, R., Rick, C., Hernandez-Lopez, S., Laville, J.A., Guzman, J.N., Galarraga, E., Surmeier, D.J., and Bargas, J. (2003). Spontaneous voltage oscillations in striatal projection neurons in a rat corticostriatal slice. J. Physiol. *553*, 169–182.

Waters, J., Larkum, M., Sakmann, B., and Helmchen, F. (2003). Supralinear Ca^{2+} influx into dendritic tufts of layer 2/3 neocortical pyramidal neurons in vitro and in vivo. J. Neurosci. *23*, 8558–8567.

Wilson, C.J. (1998). Basal ganglia. In The Synaptic Organization of the Brain, G.M. Shepherd, ed. (New York: Oxford University Press), pp. 329–375.

Wilson, C.J., and Kawaguchi, Y. (1996). The origins of two-state spontaneous membrane potential fluctuations of neostriatal spiny neurons. J. Neurosci. *16*, 2397–2410.

Xu, W., and Lipscombe, D. (2001). Neuronal Ca(V)1.3alpha(1) L-type channels activate at relatively hyperpolarized membrane potentials and are incompletely inhibited by dihydropyridines. J. Neurosci. *21*, 5944–5951.

Yasuda, R., Sabatini, B.L., and Svoboda, K. (2003). Plasticity of calcium channels in dendritic spines. Nat. Neurosci. *6*, 948–955.

Yuste, R., and Denk, W. (1995). Dendritic spines as basic functional units of neuronal integration. Nature *375*, 682–684.